

IHTC14-22751

THE EFFECT OF LIQUID FILM EVAPORATION ON FLOW BOILING HEAT TRANSFER IN A MICRO TUBE

Youngbae Han, Naoki Shikazono and Nobuhide Kasagi

Department of Mechanical Engineering

The University of Tokyo,

Hongo 7-3-1, Bunkyo-ku, Tokyo, Japan

ABSTRACT

Flow boiling in micro channels is attracting large attention since it leads to large heat transfer area per unit volume. Generated vapor bubbles in micro channels are elongated due to the restriction of channel wall, and thus slug flow becomes one of the main flow regimes. In slug flow, sequential bubbles are confined by the liquid slugs, and thin liquid film is formed between tube wall and bubble. Liquid film evaporation is one of the main heat transfer mechanisms in micro channels and liquid film thickness is a very important parameter to determine heat transfer coefficient. In the present study, liquid film thickness is measured under flow boiling condition and compared with the correlation proposed under adiabatic condition. The relationship between liquid film thickness and heat transfer coefficient is also investigated. Pyrex glass tube with inner diameter of $D = 0.5$ mm is used as a test tube. Working fluids are water and ethanol. Laser focus displacement meter is used to measure the liquid film thickness. Initial liquid film thickness under flow boiling condition can be predicted well by the correlation proposed under adiabatic condition. However, measured liquid film thickness becomes thinner than the predicted values in the cases of back flow and short slugs. These are considered to be due to the change of velocity profile in the liquid slug. Under flow boiling condition, liquid film profile fluctuates due to high vapor velocity and shows periodic pattern against time. Frequency of periodic pattern increases with heat flux. At low quality, heat transfer coefficients calculated from measured liquid film thickness show good accordance with heat transfer coefficients obtained directly from wall temperature measurements.

1. Introduction

Flow boiling in micro channels is an emerging attractive method to dissipate high heat flux on electric chips. As channel size decreases, the ratio of surface area per unit volume

increases and thus superior heat and mass transfer can be obtained at the same flow rate. The characteristics of flow boiling in micro channels are quite different from those in macro channels. Correlations based on macro channels may fail to predict heat transfer performance of flow boiling in micro channels.

The effect of mass flow rate on boiling in micro channels is not still fully understood. On the other hand, there is a consensus that heat transfer coefficient is largely affected by heat flux [1]. On this trend, Lazarek and Black [2] explained that nucleate boiling is the dominant heat transfer mechanism in micro channels as in macro channels.

However, it is reported recently by several visualization experiments of flow boiling in micro channels that the evaporation of the thin liquid film formed by elongated vapor bubble suppresses nucleate boiling [3-4]. It is also reported that conduction through the evaporating thin liquid film is the dominant heat transfer mechanism for the flow boiling in micro channels [5]. Mukherjee [6] investigated the contribution of liquid film evaporation through numerical simulation under three conditions, i.e., nucleate boiling, moving evaporating meniscus and flow boiling in a micro channel. It is reported that liquid film evaporation is the primary heat transfer mechanism of flow boiling in a micro channel. Several heat transfer models for flow boiling in micro channels based on the liquid film evaporation have been proposed. Thome et al. [5] proposed three-zone model. In their model, slug flow is assumed as a flow regime. One periodic cell consists of three zones, i.e., liquid slug, thin liquid film and dry out regions. Initial liquid film thickness is one of the three unknown parameters. Kenning et al. [7] proposed confined bubble growth model. They took into account the variation of saturated pressure which was caused by vapor bubble expansion in their model. It is assumed that liquid film thickness is uniform. Model prediction showed good accordance with the experimental results.

Due to the importance of liquid film thickness, many researches have been conducted to measure the liquid film

thickness in micro tubes. Taylor [8] experimentally obtained the liquid film thickness from the difference of the bubble velocity and the mean velocity in wide range of capillary number. It is reported that the liquid film thickness increases with capillary number and reaches a certain fraction of the tube diameter. Taylor's experimental data were correlated by Aussillous and Quere [9] as a function of capillary number:

$$\frac{\delta}{D} = \frac{0.67Ca^{2/3}}{1 + 3.35Ca^{2/3}}, \quad (1)$$

where δ is liquid film thickness and D is tube diameter. Equation (1) is called Taylor's law.

Moriyama and Inoue [10] measured the liquid film thickness formed by a vapor bubble expansion in a narrow gap from the temperature change of the channel wall which was initially superheated. Their experimental data was correlated in terms of dimensionless boundary layer thickness, capillary number and Bond number as follows:

$$\frac{\delta}{D} = \begin{cases} 0.10(\delta^*)^{0.84} & (Bo > 2) \\ 0.07Ca^{0.41} & (Bo \leq 2) \end{cases}, \quad (2)$$

where δ^* is the dimensionless viscous boundary layer thickness and Bo is the Bond number based on the vapor-liquid interface acceleration. Equation (2) is employed in the three-zone model proposed by Thome et al. [5] for the initial liquid film thickness.

Han and Shikazono [11, 12] measured the local and instantaneous liquid film thickness in micro channels under adiabatic condition with laser focus displacement meter. The effect of inertial force on the liquid film thickness was investigated using micro channels with different diameters and several working fluids. Empirical correlations based on capillary number, Reynolds number and Weber number were proposed. They also investigated the effect of bubble acceleration on liquid film thickness [13]. It is observed that the increase of liquid film thickness with capillary number is restricted when bubble acceleration is large. It is explained that liquid film thickness decreases because the curvature at bubble nose and transition region is affected by flow acceleration.

Although many experiments have been carried out to measure liquid film thickness in micro tubes, most of the experiments were conducted under adiabatic condition. However, under flow boiling condition, the bubble velocity is not constant but accelerated due to phase change. Thus, it is necessary to consider how flow boiling affects the liquid film thickness. Although several models for flow boiling heat transfer in micro tubes based on liquid film evaporation are proposed, the effect of liquid film evaporation on flow boiling heat transfer in micro tubes is not fully understood. In the present study, liquid film thicknesses are measured under flow boiling condition and compared with those under adiabatic

condition. The relationship between liquid film thickness and heat transfer coefficient is also investigated.

2. Experimental setup and procedures

2.1 Experimental setup

Figure 1 shows the schematic diagram of the experimental setup. In Fig. 1, working fluid is degassed by the degasser and pumped at a uniform flow rate with the plunge pump. In the preheater, working fluid is heated up to the desired temperature. Pyrex glass tube of $D = 0.5$ mm inner diameter is used as a test tube. Figure 2 shows the schematic diagram of the test section. Flow direction is horizontal. Acryl blocks are used for connection and thermal insulation. Test tube is coated by ITO, which is transparent conductive film for Joule heating. ITO film is connected to the DC power supply. Total length of the test tube is 100 mm and heating length is 85 mm. Outer wall temperatures at eight positions are measured by K-type thermocouples calibrated within $\pm 0.2^\circ\text{C}$ error. Two thermocouple probes and two pressure sensors are used to measure the temperatures and pressures at the inlet and the outlet as shown in Fig. 2. The data for measured temperature, pressure, voltage and current are collected by data acquisition system and recorded by PC.

The velocity of the vapor bubble is measured from the images of vapor-liquid interface captured by the high-speed camera (Photron SA1.1). Frame rate varies according to the bubble velocity and increases up to 5000 frames per second. Laser focus displacement meter (LT9010M, Keyence, LFDMM hereafter) is used to measure the liquid film thickness. LFDMM has been used by several researchers for liquid film thickness measurements [11-15]. Detailed explanation and measurement uncertainties are presented in the previous paper [11]. In the present experiments, liquid film thickness at the tube side is measured. Measurement frequency is 1 kHz. Liquid film thickness measurement is synchronized with capturing the images of bubble expansion. Measured liquid film thickness is transformed to DC voltage signal in the range of $\pm 10\text{V}$. Output signal was sent to PC through GPIB interface and recorded with LabVIEW.

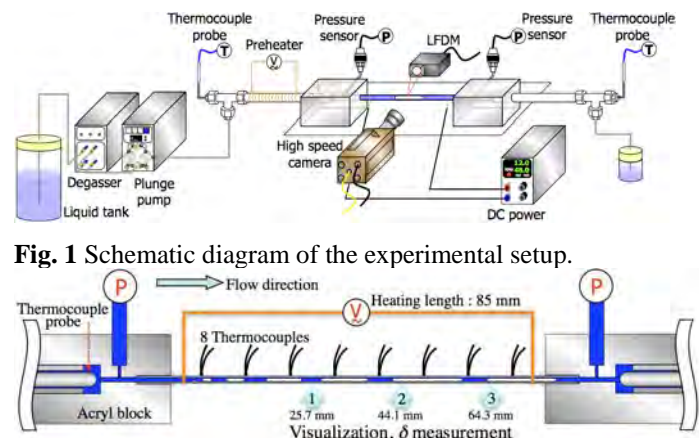


Fig. 1 Schematic diagram of the experimental setup.

Fig. 2 Schematic diagram of the test section

2.2 Experimental procedures

Two different experiments are conducted in this study. In the first part, liquid film thickness is measured under flow boiling condition without measuring the outer wall temperatures. Water and ethanol are used as working fluids. Mass flow rate is fixed at $G = 169 \text{ kg/m}^2\text{s}$. Inlet temperature is increased up to saturated temperature and small vapor bubbles generated in the preheater are introduced to the test section. Vapor bubbles expand in the test section and bubble velocity increases due to liquid film evaporation. Because of the flow instability, bubble velocity and acceleration show variations under the same mass flow rate and heat flux. Liquid film thickness is measured with different heat fluxes. Liquid film thickness is measured at two different positions $z = 25.7 \text{ mm}$ and 64.3 mm , where z is the distance from the starting point of heating as shown in Fig.2.

In the second part, the relationship between liquid film thickness and heat transfer coefficient is investigated by measuring outer wall temperatures. In order to reduce heat loss, whole test tube is covered with thermal insulator except for the small area where liquid film thickness is measured by LFDM. Only water is used as a working fluid for the second part. Inlet temperature is controlled as $T_{\text{inlet}} = 90 \text{ }^\circ\text{C}$. Mass flow rates are $G = 169, 254$ and $381 \text{ kg/m}^2\text{s}$ and heat flux is ranged from 77 kW/m^2 to 735 kW/m^2 . Liquid film thickness is measured at three different positions $z = 25.7, 44.1$ and 64.3 mm as shown in Fig. 2. Temperatures, pressures, voltage and current are measured with a measurement frequency of 1 Hz . After steady state is reached, 20 data points are averaged and used for the subsequent data reduction.

2.3 Experimental data reduction

Heat flux to the working fluid is calculated as follows:

$$q''(z) = \frac{VI}{L \cdot \pi D_{\text{in}}} - q''_{\text{loss}}(z), \quad (3)$$

$$q''_{\text{loss}}(z) = h_{\text{loss}}(z) \cdot (T_{\text{wall_out}} - T_{\text{air}}), \quad (4)$$

where $q''(z)$ is local heat flux, V is voltage, I is current, L is heating length, D_{in} is inner diameter and $q''_{\text{loss}}(z)$ is local heat loss. Local natural convection heat transfer coefficient $h_{\text{loss}}(z)$ is obtained from the heat loss experiment conducted prior to the boiling experiment. $T_{\text{wall_out}}$ and T_{air} are temperatures of outer wall and air, respectively. Inner wall temperatures are calculated from the one dimensional heat conduction equation as follows:

$$T_{\text{wall_in}} = T_{\text{wall_out}} - \frac{q''(z) D_{\text{in}}}{k} \ln\left(\frac{D_{\text{out}}}{D_{\text{in}}}\right), \quad (5)$$

where k is the thermal conductivity of Pyrex glass. Under flow boiling condition, heat transfer coefficient is calculated as:

$$h(z) = \frac{q''(z)}{T_{\text{wall_in}} - T_{\text{sat}}(z)}, \quad (6)$$

where $T_{\text{sat}}(z)$ is local saturated temperature. Local saturated temperature varies along the test channel due to the pressure drop. The test tube consists of subcooled and saturated regions and thus the whole length of the test tube can be decomposed as:

$$L_{\text{total}} = L_{\text{sub}} + L_{\text{sat}}, \quad (7)$$

If we assume that the bulk temperature at $z = L_{\text{sub}}$ to be the saturated temperature T_{sat} . L_{sub} is obtained from the energy balance equation as:

$$L_{\text{sub}} = \frac{C_p \cdot G \cdot D_{\text{in}}}{4q''} (T_{\text{sat}}(L_{\text{sub}}) - T_{\text{inlet}}) \quad (8)$$

The pressure loss ΔP_{sub} can be calculated from L_{sub} as follows:

$$\Delta P_{\text{sub}} = f \frac{1}{2} \rho U^2 \frac{L_{\text{sub}}}{D_{\text{in}}}, \quad (9)$$

where f , ρ and U are the friction factor of the laminar Poiseuille flow, the liquid density and the bulk mean velocity, respectively. The saturation pressure at $z = L_{\text{sub}}$ is then given as follows:

$$P(L_{\text{sub}}) = P_{\text{in}} - \Delta P_{\text{sub}}, \quad (10)$$

where P_{in} is the inlet pressure. Saturated temperature T_{sat} is obtained from Eq. (10). Saturated temperature T_{sat} is obtained from Eqs. (7)-(10) by iteration. For the saturated region, it is assumed that pressure decreases linearly. Local saturated pressure is then calculated as follows:

$$P(z) = P_{\text{inlet}} - \Delta P_{\text{sub}} - \frac{z - L_{\text{sub}}}{L - L_{\text{sub}}} (P_{\text{inlet}} - \Delta P_{\text{sub}} - P_{\text{outlet}}), \quad (11)$$

Local saturated temperature can be obtained from local saturated pressure and heat transfer coefficient is obtained from Eq. (6).

3. Experimental results and Discussion

3.1 Liquid film thickness under flow boiling condition

Han and Shikazono [13] proposed an experimental correlation for the initial liquid film thickness in a micro tube under adiabatic condition as follows:

$$\frac{\delta_0}{D} = \min \left[\left(\frac{\delta_0}{D} \right)_{\text{steady}}, \left(\frac{\delta_0}{D} \right)_{\text{accel}} \right] \quad (12)$$

where subscripts steady and accel represent steady and accelerated conditions. Each correlation is expressed as follows:

$$\left(\frac{\delta_0}{D} \right)_{\text{steady}} = \frac{0.670Ca^{2/3}}{1 + 3.13Ca^{2/3} + 0.504Ca^{0.672}Re^{0.589} - 0.352We^{0.629}} \quad (Re < Re_{\text{critical}}) \quad (13)$$

$$\left(\frac{\delta_0}{D} \right)_{\text{accel}} = \frac{0.968Ca^{2/3}}{Bo_{\text{accel}}^{0.414} + 4.838Ca^{2/3}} \quad (Bo_{\text{accel}} = \rho a D^2 / \sigma) \quad (14)$$

where δ_0 , ρ , a and σ are initial liquid film thickness, liquid density, bubble acceleration and surface tension, respectively. Equation (13) is valid only for laminar flow and liquid film thickness becomes constant for turbulent flow. Re_{critical} is critical Reynolds number at which flow changes from laminar to turbulent. $Re_{\text{critical}} = 2000$ is used in Ref. [13].

Figure 3 shows the variation of liquid film thickness during the vapor bubble expansion period. After bubble nose passes by the measurement position, liquid film is formed on the tube wall and the signal for the liquid film thickness is obtained. Initial quick decrease represents the transition from bubble nose to liquid film regions. In Fig. 3, unlike the adiabatic condition, liquid film thickness after transition region does not become constant but decreases due to evaporation and shows large fluctuation caused by high vapor velocity. Initial liquid film thickness δ_0 after the transition region is collected as experimental data. Figure 4 shows measured bubble velocity against time for the same condition as Fig. 3.

Figure 5 shows dimensionless liquid film thickness δ_0/D against capillary number $Ca = \mu U / \sigma$ for the experiments using ethanol. Dotted line is the Taylor's law, Eq. (1). Highly viscous fluid is used and the effects of inertial force and acceleration are neglected in Eq. (1). Solid line is the prediction line using Eq. (13) at $Re_{\text{critical}} = 2000$. At small capillary number, liquid film thickness follows the prediction under steady condition, Eq. (13). It is reported that the effects of inertial force and acceleration are negligible at small capillary numbers [13]. However, as capillary number increases, measured liquid film thickness is smaller than Eq. (13) and shows large variation.

In Fig. 6, measured liquid film thicknesses under flow boiling condition are compared with the predicted values using Eq. (12). As can be seen from Fig. 6, Eq. (12) can predict liquid film thickness under flow boiling condition relatively well within $\pm 15\%$ error. It is observed that experimental values become larger than the prediction at larger heat flux. As heat flux increases, nucleation and bubble expansion become more active and this results in the increase of the bulk liquid flow velocity, which makes liquid film thicker. It is considered that this underestimation is attributed to the initial velocity profile in the liquid slug. Equation (14) is obtained from the experiment where flow was accelerated from stationary condition [13].

Figure 7 is the schematic of the velocity profiles under accelerated condition with different initial velocity conditions. As shown in Fig. 7, velocity profile depends on its initial profile. It is considered that this initial velocity profile difference affects the curvature at the bubble nose and transition region, which changes the liquid film thickness.

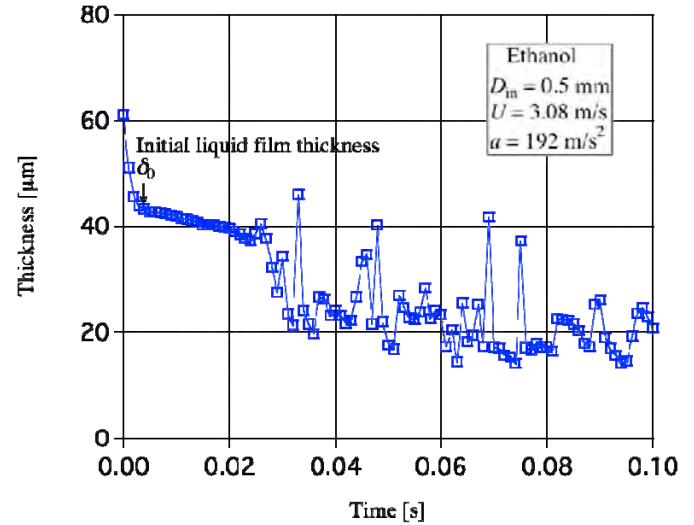


Fig. 3 Time variation of liquid film thickness using saturated ethanol.

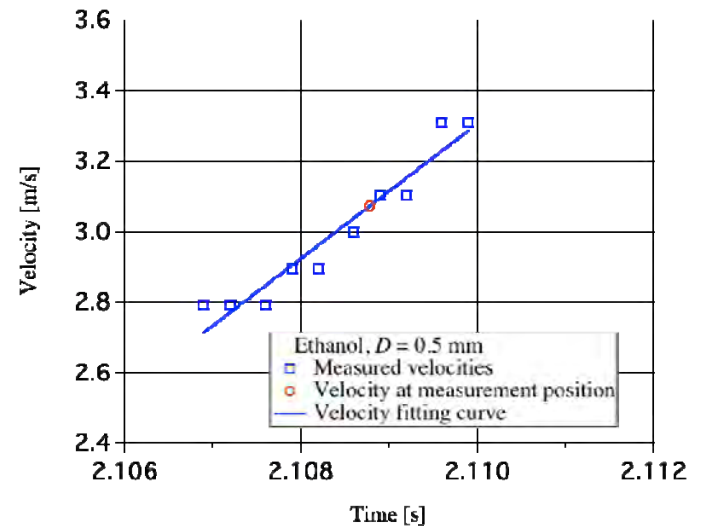


Fig. 4 Measurement bubble velocity against time for the same condition of Fig. 3, $U = 3.08$ m/s and $a = 192$ m/s².

Figure 8 shows the dimensionless liquid film thickness δ_0/D against capillary number $Ca = \mu U / \sigma$ for the experiments using water. Dashed line is the prediction using Eq. (13) at $Re_{\text{critical}} = 2000$. Unlike the case of ethanol, liquid film thickness is thicker than Eq. (13) at $Re_{\text{critical}} = 2000$. It is considered that under accelerated condition, liquid flow is still laminar even for $Re > 2000$. In Fig. 8, solid line is the prediction line of Eq. (13) using $Re_{\text{critical}} = 4300$. It can be seen that measured liquid film

thickness follows solid line at small capillary number, $Ca < 0.01$. As the trend for ethanol, liquid film thickness data for water show large variation.

Figure 9 shows comparison between measured liquid film thickness and predicted values by Eq. (12) for flow boiling experiment using water. Equation (12) can also predict liquid film thickness of water relatively well within $\pm 15\%$ error. As the trend shown in Fig. 6 for ethanol, liquid film thickness of saturated water becomes thicker than the prediction as heat flux increases.

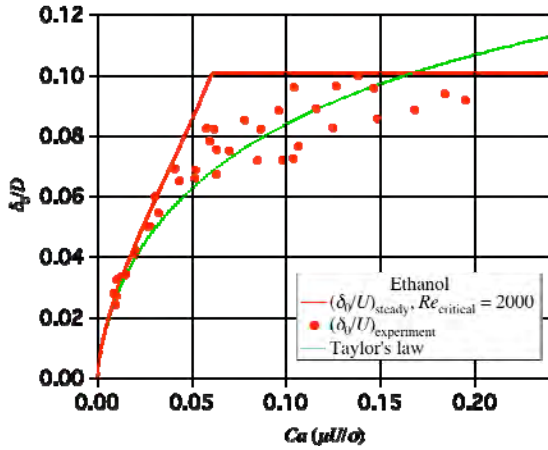


Fig. 5 Dimensionless liquid film thickness δ_0/D against capillary number $Ca = \mu U/\sigma$ for the experiment using ethanol.

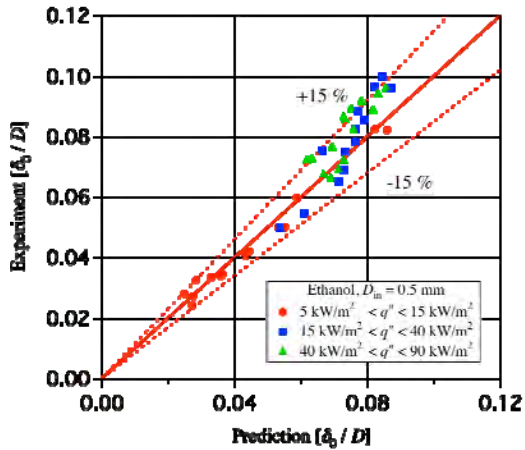


Fig. 6 Comparison between measured liquid film thickness and predicted values by Eq. (12) for flow boiling experiment using ethanol.

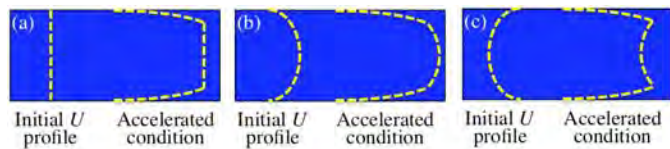


Fig. 7 Effect of initial liquid velocity profile under accelerated condition.

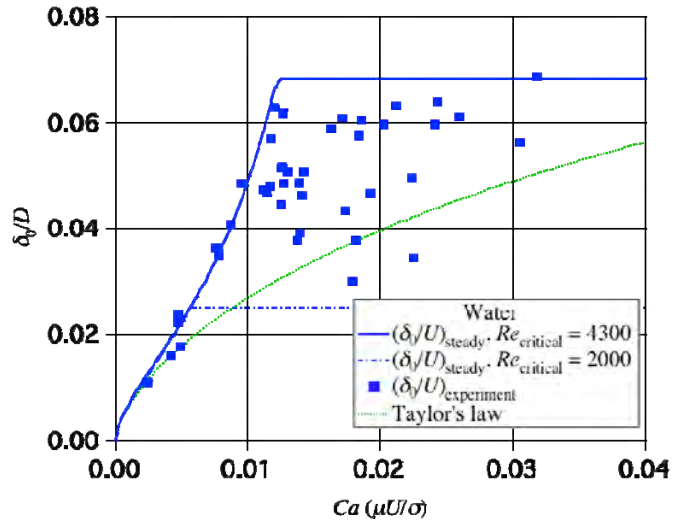


Fig. 8 Dimensionless liquid film thickness δ_0/D against capillary number $Ca = \mu U/\sigma$ for the experiment using water.

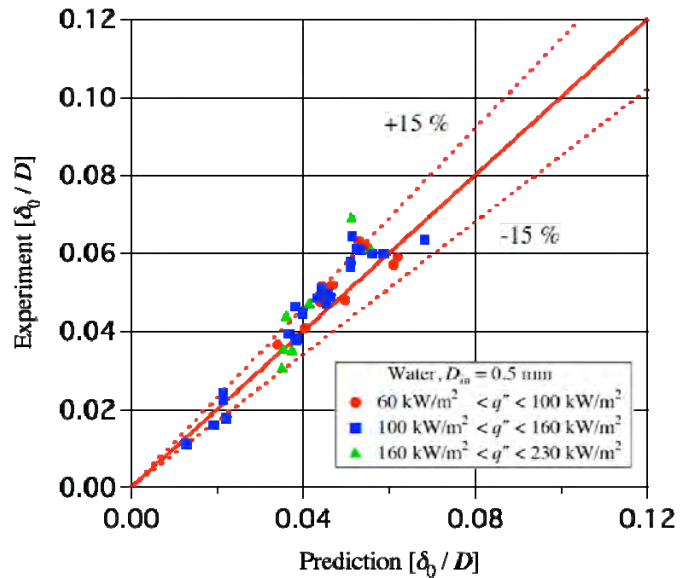


Fig. 9 Measured liquid film thickness against predicted values with Eq. (12) for flow boiling experiment using water in $D_{in} = 0.5$ mm.

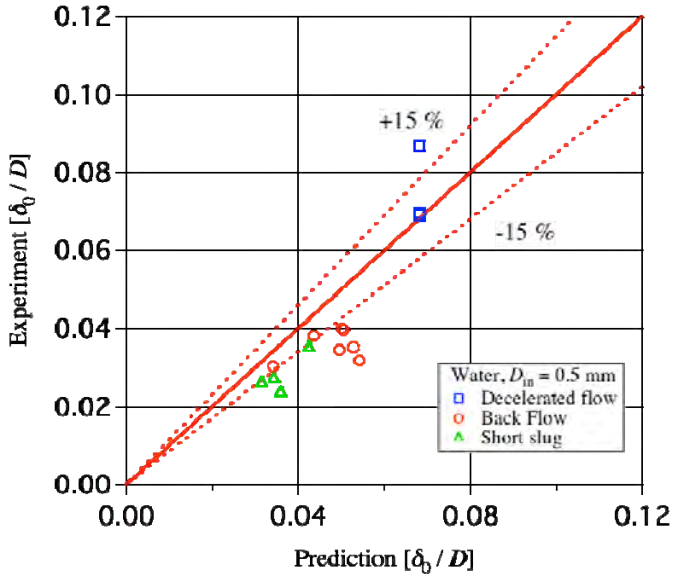


Fig. 10 Three irregular cases under flow boiling condition for the experiments using water.

Figure 10 shows some irregular cases which are not considered when Eq. (12) was developed. In the case of water, density ratio of vapor and liquid phases is much larger than that of ethanol. In micro tubes, vapor bubble is not generated unless wall superheat becomes very high. Vapor bubble expands explosively under such condition. This results in large pressure fluctuation and back flow. Such conditions correspond to the short slug, decelerated flow and back flow.

Under flow boiling condition, liquid slug length between two vapor bubbles decreases due to evaporation. In the present experiment, liquid film behind short liquid slug is thinner than those after longer slugs as shown in Fig. 10. Fujioka and Grotberg [16] numerically investigated the effect of liquid slug length on the two-phase flow in a 2D channel using finite volume scheme. It is reported that for sufficiently short liquid slugs, fluid inertia causes significant interaction between leading and trailing bubbles. In their simulation, velocity profile in short liquid slug is not parabolic but is almost flat at the channel center. It is considered that this resembles the accelerated flow case as shown in Fig. 7 (a).

Bubble velocity is sometimes decelerated because of the expansion of the preceding bubble. Under decelerated condition, Eq. (14) cannot be used because Bo_{accel} becomes negative. Therefore, liquid film thickness is compared only with Eq. (13). As shown in Fig. 10, Eq. (13) can predict liquid film thickness under decelerated condition relatively well. When flow is decelerated, velocity profile at the tube center initially keeps the original form and only the flow velocity near the wall is decelerated. This condition is similar to Fig. 7 (b). Although velocity profile is different from that under steady condition, liquid film thickness follows the correlation under steady condition, Eq. (13).

In the case of back flow, liquid film thickness becomes thinner than the predicted value. When back flow occurs, the direction of accelerated bubble is opposite to the main flow. Therefore, the variation of velocity profile near the wall becomes very large as shown in Fig. 7 (c). It is considered that the effect of surface tension is intensified, which makes liquid film thinner. Further extensive research is necessary to understand the quantitative effect of initial velocity profile on the liquid film thickness.

3.2 The effect of liquid film evaporation on heat transfer

3.2.1 Single-phase experiment

Before taking the boiling heat transfer data, present experimental setup is validated by the single-phase heat transfer experiment. Single phase Nusselt number is calculated as follows:

$$Nu = \frac{h \cdot D_{in}}{k} = \frac{D_{in}}{k} \frac{q''(z)}{(T_{wall,in} - T_{bulk})}, \quad (15)$$

$$T_{bulk} = T_{inlet} + \frac{4q''(z) \cdot z}{C_p \cdot G \cdot D_{in}}, \quad (16)$$

where C_p is specific heat. Figure 11 shows the comparison between experimental and theoretical Nusselt numbers. Experimental data show good accordance with the theoretical line.

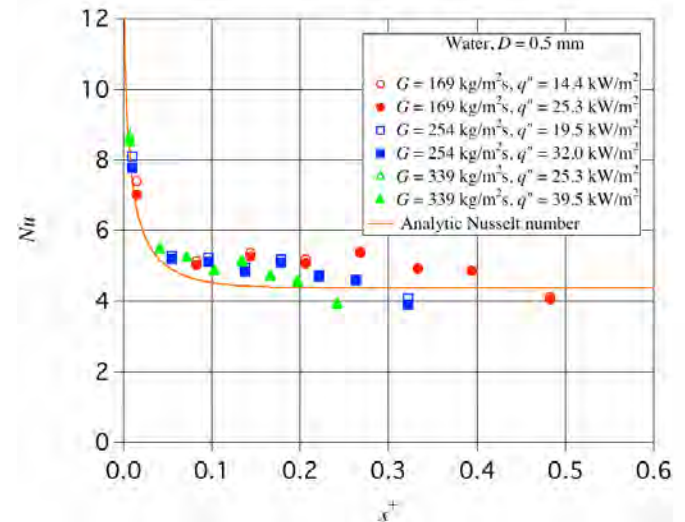


Fig. 11 Comparison between Nusselt number obtained from the present experimental setup and theoretical Nu number.

3.2.2 Periodic pattern of liquid film thickness

Figure 12 shows the time variation of liquid film thickness at $z = 64.3$ mm, for $G = 169$ kg/m²s. Liquid film thickness shows periodic pattern. The frequencies of periodic patterns

increase as heat flux increases. Vapor bubble is not generated until liquid is superheated which results in abrupt bubble expansion and thus liquid film is formed by back flow in some cases. After liquid film is formed on the wall, liquid film thickness quickly decreases with large fluctuation due to strong evaporation. However, as liquid film thickness further decreases, fluctuation becomes smaller and liquid film becomes very stable. As heat flux increases above $q'' = 187 \text{ kW/m}^2$, flow regime transits from slug flow to annular flow and becomes more unstable. Even for such cases, time variation of liquid film thickness still shows weak periodicity. As heat flux increases more than $q'' = 261 \text{ kW/m}^2$, dry out region appears.

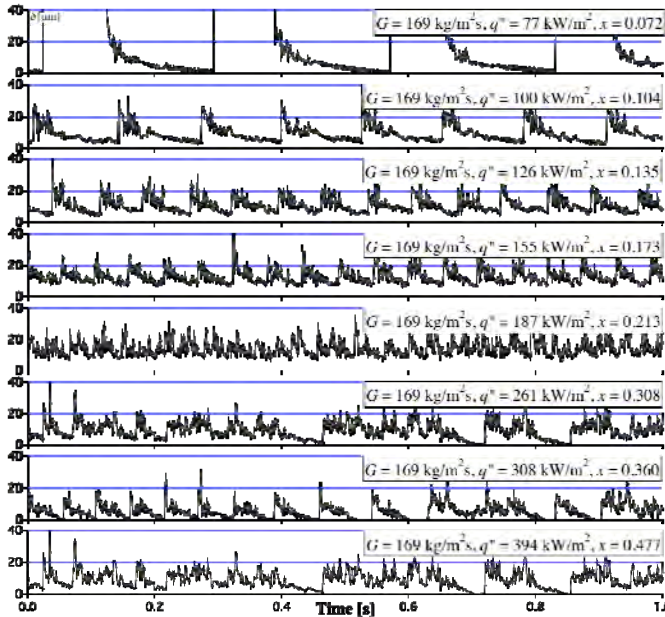


Fig. 12 Time variation of liquid film thickness with different heat fluxes at $l = 64.3 \text{ mm}$, 3rd measurement position for $G = 169 \text{ kg/m}^2\text{s}$.

3.2.3 Heat transfer coefficient

Local heat transfer coefficient can be obtained from the measured outer wall temperatures according to Eq. (6). Figure 13 shows the local heat transfer coefficient against quality at $G = 169 \text{ kg/m}^2\text{s}$. Obtained heat transfer coefficients show typical trend of flow boiling heat transfer in micro tubes reported in the review paper [1]. At quality around $x = 0.1$, heat transfer coefficient takes a maximum value. As quality increases, heat transfer coefficient decreases. It is considered that vapor bubbles are generated at $x \approx 0.1$. Vapor bubble expands both upstream and downstream. Very thin liquid film is formed near the nucleation site since flow velocity is slow. Liquid film becomes thicker as vapor-liquid interface is accelerated. In Fig. 13, maximum heat transfer coefficient decreases as heat flux increases. Liquid film near the nucleation site evaporates in a short time and tube wall is easily dried out.

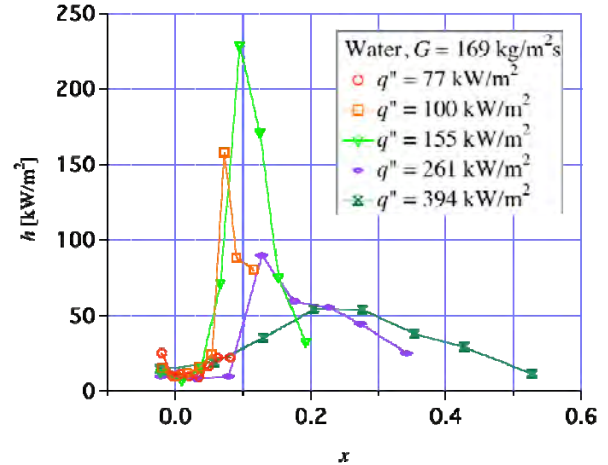


Fig. 13 Local heat transfer coefficient against quality for water and $G = 169 \text{ kg/m}^2\text{s}$.

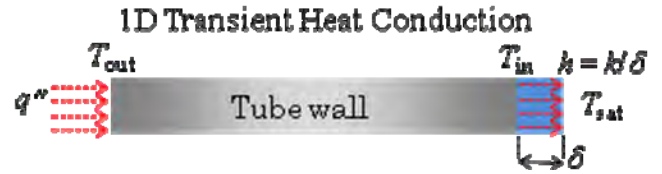


Fig. 14 Schematic diagram for one dimensional transient heat conduction.

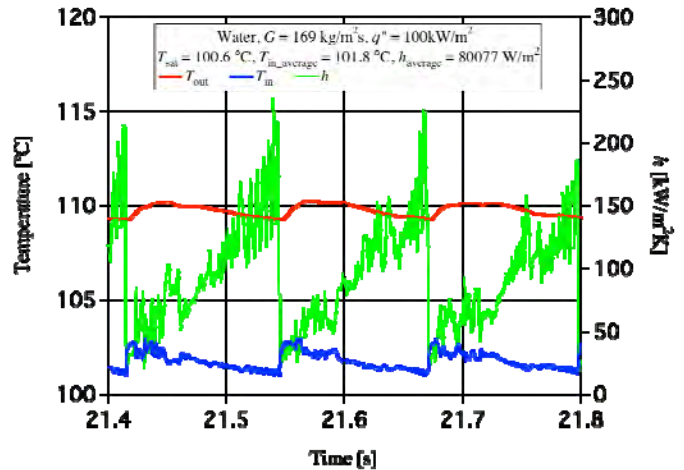


Fig. 15 Time variation of inner wall and outer wall temperatures simulated from the measured liquid film thickness.

As heat flux increases liquid film evaporates in a shorter time and dryout continues longer, which results in the decrease of heat transfer coefficient.

Outer and inner wall temperatures can be simulated from the measured liquid film thickness. Figure 14 shows the schematic diagram for one dimensional transient heat conduction in the test tube wall. In the present study, axial heat conduction is neglected. The effect of axial heat conduction on

heat transfer coefficient is usually determined by axial conduction number M as follows:

$$M = \left(\frac{k_{wall}}{k_L} \right) \left(\frac{D_{out}^2 - D_{in}^2}{D_{in} L} \right) \frac{1}{RePr}, \quad (17)$$

where k_{wall} , k_L and Pr are wall thermal conductivity, liquid thermal conductivity and Prandtl number, respectively. It is reported that if $M > 10^{-2}$ axial heat conduction should be considered [17]. In the present study, $M < 3.0 \times 10^{-4}$ for all experimental cases. Thus, one dimensional heat conduction assumption is reasonable.

Local saturated temperature T_{sat} is obtained from Eqs. (7)-(11), and it is assumed that the vapor-liquid interface temperature is equal to saturated temperature. Heat flux is also given as Eqs. (3)-(4). If we assume linear temperature gradient

in the liquid film, heat transfer coefficient h on the inner wall is determined as follows:

$$h = k_L / \delta. \quad (18)$$

Uniform heat flux q'' at the outer wall and Eq. (18) for the inner wall are given as boundary conditions. Giving the vapor-liquid interface temperature T_{sat} , outer and inner wall temperatures can be calculated.

When micro tube is filled with liquid slug, heat transfer coefficient of fully developed laminar single-phase flow is assumed. If liquid film thickness becomes thinner than $0.1 \mu\text{m}$, heat transfer coefficient is set to zero. Time step in the simulation is 0.1 ms . Liquid film thickness at each time step is linearly interpolated from the measured liquid film thickness. Figure 15 shows simulated example for $G = 169 \text{ kg/m}^2\text{s}$ and $q'' = 100 \text{ kW/m}^2$. According to the variation of heat transfer

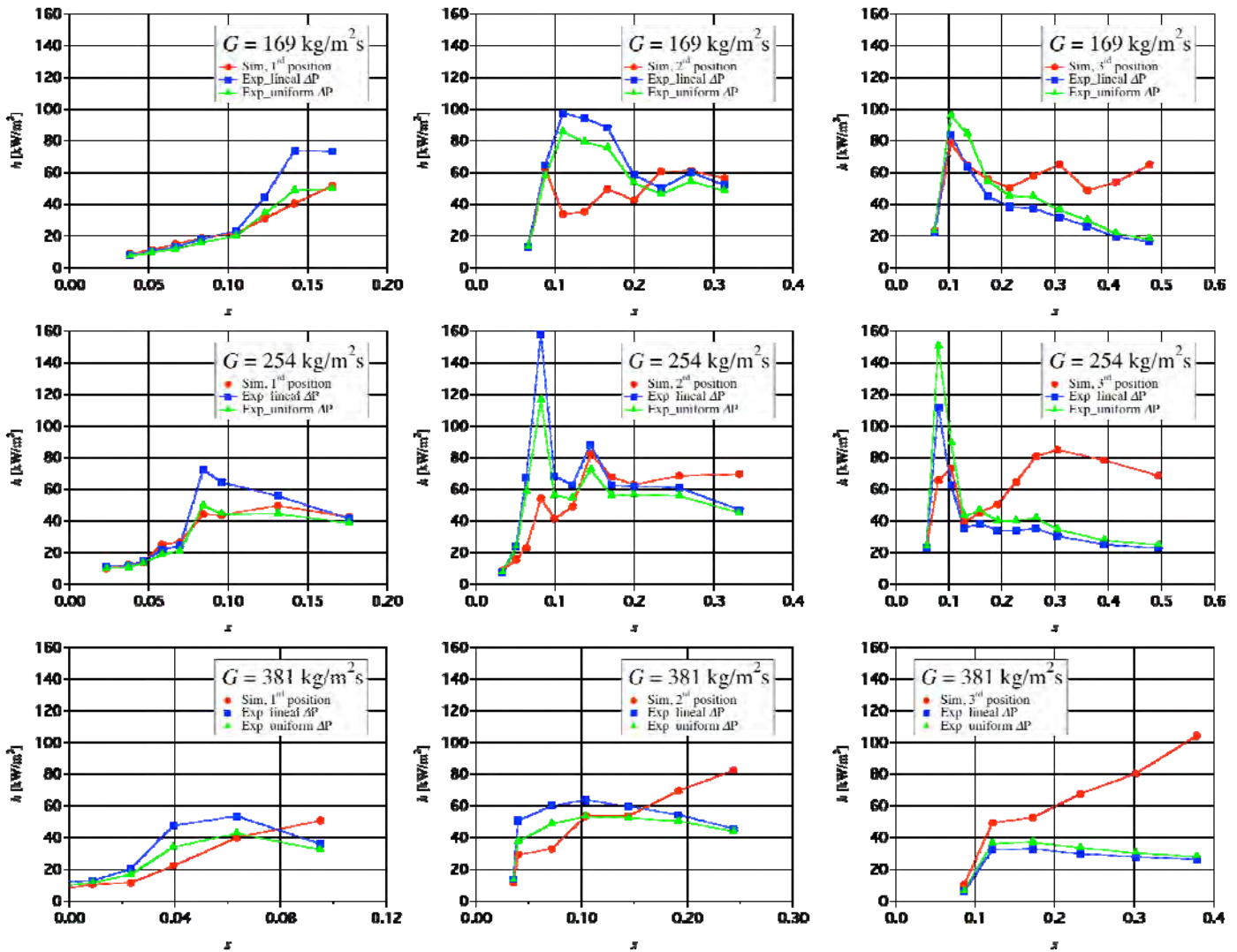


Fig. 16 Comparison between the heat transfer coefficients calculated from measured liquid film thickness and the heat transfer coefficients obtained directly from wall temperature measurements.

coefficient, outer and inner wall temperatures also show periodic variations. Liquid film thicknesses for the period of 2 seconds are used for the simulation. Finally, averaged heat transfer coefficient is obtained as follows:

$$h_{\text{average}} = q'' / (T_{\text{wall_in_average}} - T_{\text{sat}}), \quad (19)$$

where $T_{\text{wall_in_average}}$ is the averaged inner wall temperature during one period.

Figure 16 shows the comparison between the heat transfer coefficients calculated from measured liquid film thickness and those obtained directly from wall temperature measurements. Measurement position is fixed in each graph and thus increasing vapor quality means increasing heat flux. Solid circular symbols represent simulated heat transfer coefficients from liquid film thickness. Solid square symbols represent the heat transfer coefficients from wall temperature measurement using local saturated pressure under the assumption of linear pressure drop. Local saturated pressure is calculated by linear interpolation as shown in Eq. (11). Solid triangle symbols in Fig. 16 represent heat transfer coefficient using mean saturated temperature:

$$T_{\text{sat}} = T_{\text{sat}} \left(\frac{P_{\text{inlet}} + P_{\text{outlet}}}{2} \right). \quad (19)$$

Saturated temperature is assumed to be constant along the test tube in the cases of solid triangle symbols.

At small quality, heat transfer coefficients calculated from measured liquid film thickness are in good accordance with those obtained directly from wall temperature measurement. This might be attributed to the stable flow at small heat flux. However, as quality increases, flow becomes unstable and simulated heat transfer coefficients from liquid film thickness deviates from those obtained from wall temperatures. As mass flow rate increases, deviation becomes larger. This is due to larger heat flux given to working fluid as mass flow rate increases, which results in unstable flow and large pressure fluctuation.

Figure 17 shows an example of measured inlet and outlet pressure. As shown in Fig. 17, fluctuation of the inlet pressure is very large even for relatively small heat flux. Due to the limitation of facility, the measurement frequency of pressure is 1 Hz and it is much lower than real fluctuation frequency. Considering the trend shown in Fig. 17, local saturated pressure does not decrease linearly along the test tube. When a vapor bubble expands in a micro tube, increased vapor pressure affects the whole test section. After the end of the vapor bubble expansion cycle, wall superheat decreases, thus pressure of the whole test section decreases. In Fig. 16, the predicted heat transfer coefficient from measured liquid film thickness is closer to the uniform saturated pressure result. However, deviation is still quite large. It is necessary to know the accurate time variation of saturated pressure for better prediction.

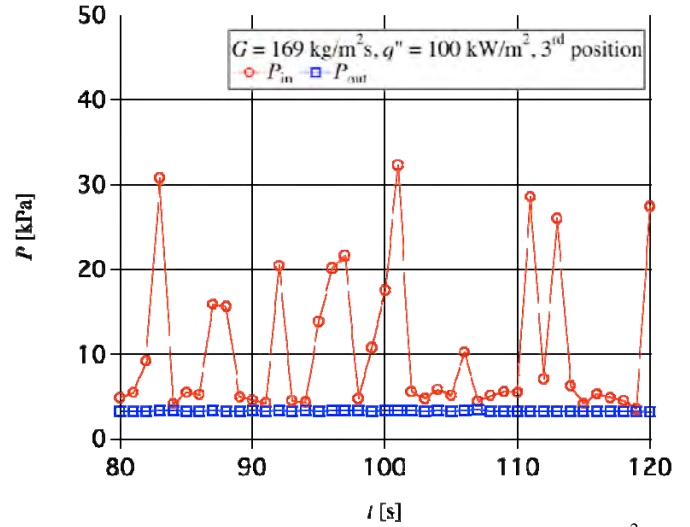


Fig. 17 Pressure fluctuation with time for $G = 169 \text{ kg/m}^2\text{s}$ and $q'' = 100 \text{ kW/m}^2$ at $z = 64.3 \text{ mm}$, 3rd measurement position.

4. Conclusions

In the present study, liquid film thicknesses are measured under flow boiling condition and compared with those under adiabatic condition. Initial liquid film thickness under flow boiling condition can be predicted relatively well by the correlation proposed under adiabatic condition. However, liquid film thickness becomes thinner than predicted values in the case of back flow and short liquid slug. This is attributed to the change of velocity profile in the liquid slug. The relationship between liquid film thickness and heat transfer coefficient is also investigated. Liquid film thickness shows periodic patterns and fluctuates due to high vapor velocity. Frequency of periodic pattern increases with heat flux. As heat flux further increases, flow becomes unstable and flow regime transits to annular flow. At small qualities, heat transfer coefficients calculated from measured liquid film thickness show good accordance with heat transfer coefficients obtained directly from wall temperature measurements.

NOMENCLATURE

Symbol	Description	Unit
Bo	Bond number	-
Ca	capillary number	-
C_p	specific heat	J/kgK
D	tube diameter	m
G	mass flow rate	kg/m ² s
h	convection heat transfer coefficient	W/m ² K
I	current	A
k	thermal conductivity	W/mK
L	heating length	m
q''	heat flux	W/m ²
Re	Reynolds number	-

T	temperature	°C
U	bubble velocity	m/s
V	voltage	V
We	Weber number	-
x	quality	-
z	distance from inlet	m

Greek Symbols

δ	liquid film thickness	m
μ	viscosity	Pa·s
ρ	density	kg/m ³
σ	surface tension coefficient	N/m

Subscripts

0	initial
in	inner
out	outer
sat	saturated
sub	subcooled

ACKNOWLEDGMENTS

We would like to thank Prof. Suzuki and Dr. Hasegawa for the fruitful discussions and suggestions. This work is supported through Grant in Aid for Scientific Research (No. 20560179) by MEXT, Japan and GCOE Mechanical System Innovation program, The University of Tokyo, Japan.

REFERENCES

- [1] Thome, J. R., 2006, "State-of-the-art overview of boiling and two-phase flows in microchannels," *Heat Transfer Engineering*, **27**, pp. 4-19.
- [2] Lazarek, G. M. and Black, S. H., 1982, "Evaporative heat transfer, pressure drop and critical heat flux in a small vertical tube with R-113," *Int. J. Heat Mass Transfer*, **25**, pp. 945-960.
- [3] Cornwell, K. and Kew, P. A., 1993, "Boiling in small parallel channels," *Energy Efficiency Process Technology*, Elsevier Appl. Science, pp 624-638.
- [4] Jacobi, A. M. and Thome, J. R., 2002, "Heat transfer model for evaporation of elongated bubble flows in microchannels," *J. Heat Transfer*, **124**, pp. 1131-1136.
- [5] Thome, J. R., Dupont, V. and Jacobi, A. M., 2004, "Heat transfer model for evaporation in micro channels. Part I: presentation of the model," *Int. J. Heat Mass Transfer*, **47**, pp. 3375-3385.
- [6] Mukherjee, A., 2009, "Contribution of thin-film evaporation during flow boiling inside microchannels," *Int. J. Therm. Sci.*, **48**, pp. 2025-2035.
- [7] Kenning, D. B. R., Wen, D. S., Das, K. S. and Wilson, S. K., 2006, "Confined growth of a vapour bubble in a capillary tube at initially uniform superheat: Experiments and modeling," *Int. J. Heat Mass Transfer*, **49**, pp. 4653-4671.
- [8] Taylor, G. I., 1961, "Deposition of a viscous fluid on the wall of a tube," *J. Fluid Mech.*, **10**, pp. 161-165.
- [9] Aussillous, P. and Quere, D., 2000, "Quick deposition of a fluid on the wall of a tube," *Phys. Fluids*, **12**, pp. 2267-2371.
- [10] Moriyama, K. and Inoue, A., 1996, "Thickness of the liquid film formed by a growing bubble in a narrow gap between two horizontal plates," *Trans. of the ASME*, **118**, pp. 132-139.
- [11] Han, Y. and Shikazono N., 2009, "Measurement of the liquid film thickness in micro tube slug flow," *Int. J. Heat Fluid Flow*, **35**, pp. 896-903.
- [12] Han, Y., Shikazono N., 2009, "Measurement of liquid film thickness in micro square channel," *Int. J. Multiphase Flow*, **30**, pp. 842-853.
- [13] Han, Y. B. and Shikazono N., 2009, "The effect of bubble acceleration on the liquid film," submitted to *Int. J. Heat Fluid Flow*.
- [14] Takamasa, T. and Kobayashi, K., 2000, "Measuring interfacial waves on film flowing down tube inner wall using laser focus displacement meter," *J. Multiphase Flow*, **26**, pp. 1493-1507.
- [15] Hazuku, T., Fukamachi, N., Takamasa, T., Hibiki, T. and Ishii, M., 2005, "Measurement of liquid film in microchannels using a laser focus displacement meter," *Experiments in Fluids*, **38**, pp. 780-788.
- [16] Fujioka, H. and Grotberg, J. B., 2004, "Steady propagation of a liquid plug in a two-dimensional channel," *ASME Journal of Biomechanical Engineering*, **126**, pp. 567-577.
- [17] Marazana, G., Perry, I. And Maillet, D., 2004, "Mini- and Micro-channels: Influence of Axial Conduction in the Walls," *Int. J. Heat Mass Transfer*, **47**, pp.3993-4004.